Nanogold: A Quantitative Phase Map

Amanda S. Barnard,[†,*] Neil P. Young,[‡] Angus I. Kirkland,[‡] Marijn A. van Huis,[§] and Huifang Xu[⊥]

[†]CSIRO Materials Science & Engineering, Clayton, 3168, Australia, [‡]Department of Materials, University of Oxford Parks Road, Oxford, OX1 3PH, U.K., [§]Kavli Institute of Nanoscience, Delft University of Technology Lorentzweg 1, 2628 CJ Delft, The Netherlands, and [⊥]Department of Geology and Geophysics, and Materials Science Program University of Wisconsin—Madison, Madison, Wisconsin 53706

ABSTRACT The development of the next generation of nanotechnologies requires precise control of the size, shape, and structure of individual components in a variety of chemical and engineering environments. This includes synthesis, storage, operational environments and, since these products will ultimately be discarded, their interaction with natural ecosystems. Much of the important information that determines these properties is contained within nanoscale phase diagrams, but quantitative phase maps that include surface effects and critical diameter (along with temperature and pressure) remain elusive. Here we present the first quantitative equilibrium phase map for gold nanoparticles together with experimental verification, based on relativistic *ab initio* thermodynamics and *in situ* high-resolution electron microscopy at elevated temperatures.

KEYWORDS: gold · nanoparticles · shape · phase diagram · thermodynamics · modeling

Nanoparticles of gold are currently attracting considerable attention for use in biomedical applications including drug delivering, heating, sensing,[1] and in nanocatalysis.[2] However, our ability to control the properties upon which these applications are based is still intrinsically linked to the nanomorphology of individual particles.

Most theoretical models predict that, in general, the more perfect the nanoparticles, the better they perform. However, real nanoparticles are rarely crystallographically ideal, and planar defects such as contact twins and intrinsic or extrinsic stacking faults, form during growth in materials with low stacking fault or twin boundary energy, and surface energy anisotropy.[3] Gold features in this group, often exhibiting structural and morphological modifications including single or multiple (parallel, contact) twinning[4] and cyclic twinning resulting in decahedral[5] and truncated decahedral structures[6] (Figure 1). The observation of decahedral structures, often referred to as multiply twinned particles or MTPs, are particularly interesting, due to their unusual, crystallographically forbidden 5-fold (pentagonal) symmetry and concomitant lattice strain at small sizes.[7] These are distinct from larger MTPs characterized by large fcc domains with a dislocation core. The relative stability between these structural motifs has been the focus of much attention,[8] but from a technological standpoint the key question is what the stable structure of a gold nanoparticle will be postsynthesis in realistic engineering and natural environments.

An exceptional way of capturing the essential information about the structural stability of gold nanoparticles under a range of conditions is to consult a nanoscale phase diagram, which provides a powerful, predictive map of chemical equilibrium. In general, a phase diagram (or map) identifies the thermodynamically stable structure of a material at a given temperature (T), composition (C), and/or pressure (P), but the development of nanoscale phase diagrams with an additional dimension representing the critical diameter (D) has been slow. Ideally in addition to size, a useful quantitative nanoscale phase map for gold should distinguish between structural motifs and shapes, as above, since the shape is fundamentally linked to important properties including reactivity[2] and surface plasmon resonances.[9] The high temperature region of the nanogold phase diagram has been explored experimentally by Koga et al., but only the relationship between structural motif and the melting transition was firmly established.[10] Using classical molecular dynamics on a limited set of small structures, a *qualitative* phase map for gold nanoparticle has been previously suggested by Kuo and Clancy,[11] but is in disagreement with other earlier empirical attempts.[12] A phase map of this type could also be generated by

*Address correspondence to amanda.barnard@csiro.au.

Received for review March 5, 2009 and accepted May 13, 2009.

Published online June 2, 2009.
10.1021/nn900220k CCC: $40.75

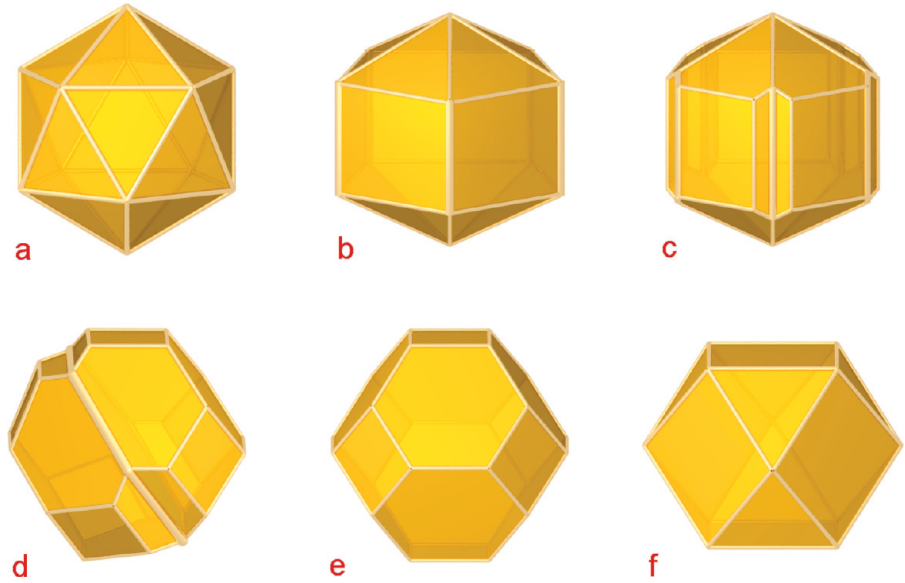

Figure 1. Various shapes exhibited by gold nanoparticles: the Mackay icosahedron (a), the Ino (b) and Marks (c) decahedra, the symmetrically twinned truncated octahedron (d), the ideal truncated octahedron (e), and the ideal cuboctahedron (f).

comparing the Gibbs free energy of formation (G) of all possible motifs, as a function of size, temperature, and pressure, and theoretical modeling is proving to be a very useful tool in this regard.

Gold is currently at the forefront of theoretical and experimental nanoscience, and various robust methodologies for treating gold nanoparticles have been firmly established.[8,13,14] Rather than treating each type of shape and structure explicitly, *via* individual computer simulations, the approach in this paper involves a multiscale model used to examine the equilibrium shape of crystals *via* the convex envelope of planes (perpendicular to the surface normals) that minimizes surface energy for a given enclosed volume. The advantages of this type of thermodynamic modeling include the ability to compare nonequilibrium shapes, to optimize the morphology with respect to experimentally relevant parameters such as size, temperature, or surface chemistry (or chemical potential), and to use relativistic first principle methods to consider (with relative ease) nanoparticles at sizes inaccessible to all but atomistic level simulations without necessitating a prohibitively large number of explicit simulations of individual structures.

THE QUANTITATIVE NANOGOLD PHASE MAP

We have used this efficient theoretical approach based on relativistic *ab initio* calculations (see Methods) to model the free energy of formation for *all* shapes and motifs illustrated in Figure 1, and have compared the results to determine the lowest energy morphology as a function of size D. The results for the truncated octahedral fcc motif (Figure 1e), the Marks decahedron (Figure 1c) and the Mackay icosahedron (Figure 1a) are shown in Figure 2a at $T = 0$ K. In this example crossovers that indicate a change in the thermodynamically favored motif are highlighted, showing the change from an icosahedron to a decahedron at A, and the change from a decahedron to truncated octahedron at B.

By repeating this procedure at different temperatures, we have been able to ascertain the temperature dependence of the crossover sizes. Figure 2b contains the same exemplary set of motifs at $T = 300$ K. An important aspect of this type of modeling, and an advantage it has over alternative approaches, is the optimization of the nanoparticle shape at each point in the $\langle T,D \rangle$ manifold. It has previously been shown that the ratio of {111} to {100} surface area is proportional to the temperature, and this behavior must be included in the thermodynamic modeling if the fcc structures are to be adequately described.

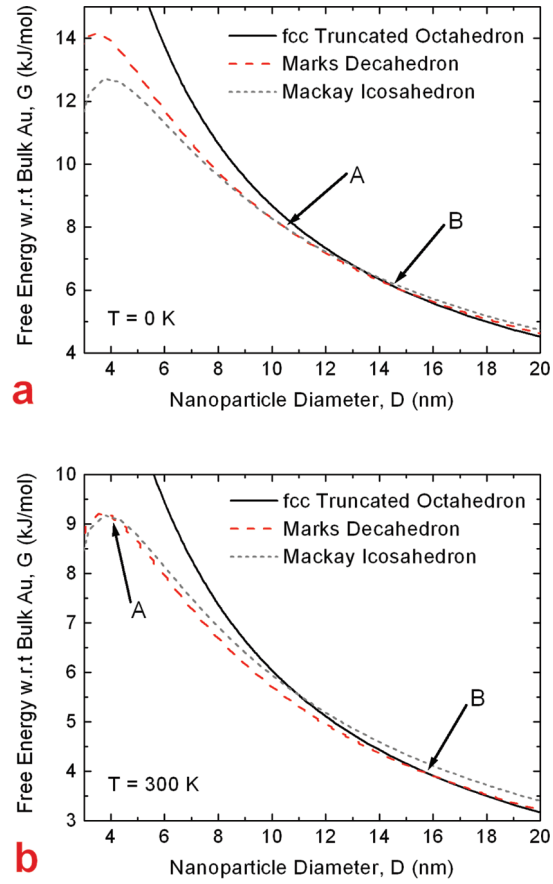

Figure 2. Comparison of the free energy of truncated octahedral (fcc), Mackay icosahedral and Marks decahedral structural motifs, at (a) $T = 0$ K and (b) $T = 300$ K. The icosahedral to decahedral (A) and decahedral to fcc (B) transformation sizes are marked.

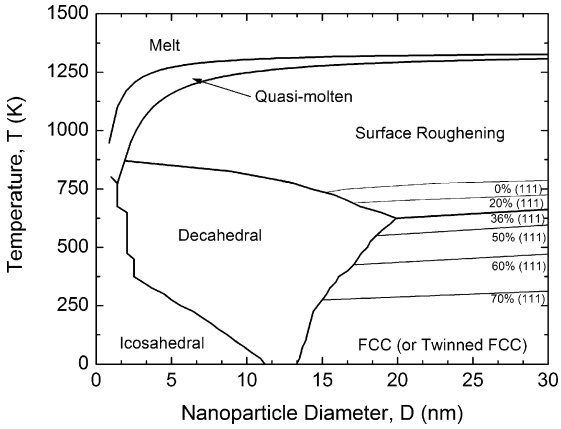

Figure 3. Quantitative phase map of gold nanoparticles, based on relativistic first principles calculations.

Once the free energy is determined for each (optimized) structure, this procedure ultimately provides a matrix of structural data in $\langle T,D \rangle$ space and thus allows the construction of the first *quantitative* nanoscale phase map of gold, based on relativistic first principles (Figure 3). At low temperatures this diagram maps the thermodynamically stable size and temperature range for each motif, and includes the isomorphs that predict the shape of fcc particles in the truncated octahedron−cuboctahedron continuum. More generally, Figure 3 predicts the (low temperature, isothermic) structural order of the icosahedral < decahedral < fcc structures, in agreement with previous selective studies examining their stability at different sizes.[13]

At higher temperatures, the model predicts the onset of different types of melting behavior. In particular, the upper boundary of the map features a size dependent melting transition. This has been calculated using the formalism of Qi and Wang,[15] which accounts for differences in the shape of individual particles. The upper boundary represents the size- (and shape-) dependent melting transition for an icosahedral particle, and the lower boundary represents the same transition in decahedral and cuboctahedral nanoparticles (which are almost energetically indistinguishable). Between them lies a "quasi-molten" region, where decahedral and fcc particles will be sufficiently fluid so as to adopt the icosahedral motif (before melting). It may be thought of as a molten/icosahedral coexistence region and is well-known from explicit molecular dynamics simulations reported by others.[11] Beneath the quasi-molten region is a region of the phase-map denoted as "surface roughening". As the name suggests, this region contains nanoparticles that have an underlying crystalline core-structure but exhibit a deterioration of the surface structure. This includes surface melting, the formation of (solid) amorphous-like gold shells, or a sufficient density of surface defects such that it can no longer be classified as fcc gold. In this region, fcc-cores and decahedral-cores are energetically indistinguishable within the resolution of the model. This feature is a direct consequence of the theoretical description of the critical temperature[15] which includes the size-dependent surface melting. As the temperature is increased we surpass the surface melting temperature well before we reach the corresponding bulk melting temperature, which gives rise to this region on the map. This phenomenon has routinely been observed during high-temperature molecular dynamics simulations[11] examining the melting[16] and crystallization[17] of gold nanostructures of various sizes and has been observed in a metal alloy during the elegant experiments of Sutter and Sutter.[18]

The above methodology is an invaluable predictive tool for probing nanoparticle structures without recourse to extensive experimental classification, and for anticipating how the structure of gold nanoparticles will respond to external perturbations. However, when referring to a phase-map of this type, it is important to

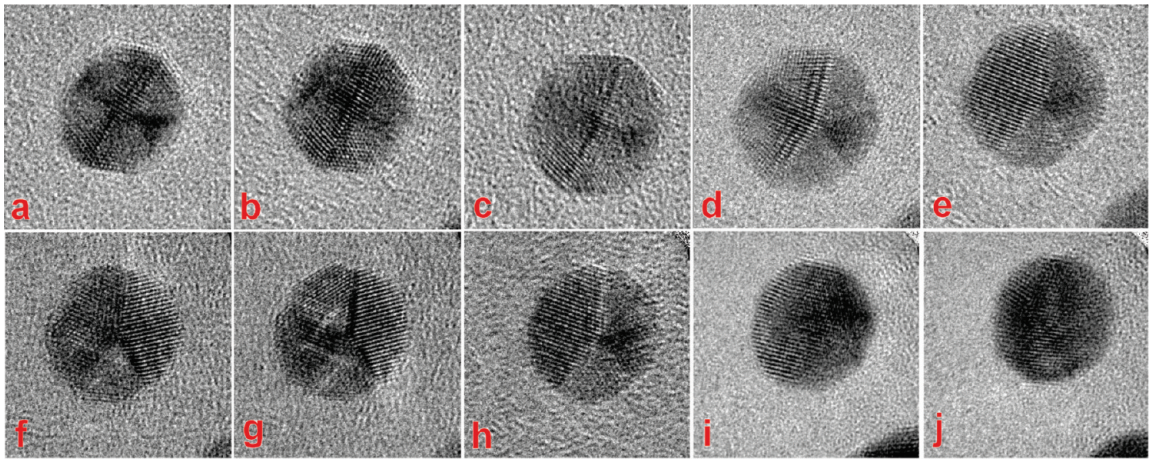

Figure 4. Representative images taken from a series of HRTEM data of a Au nanoparticle recorded as a function of temperature. The average nanoparticle diameter is ~7.5 nm. Initial icosahedral structure (close to a ⟨112⟩ projection) at (a) 300 (room temperature), (b) 500, (c) 650, (d) 700 (the structure transforms to a decahedral morphology at close to a ⟨110⟩ projection), (e) 750 K. The temperature is then reduced back to room temperature (f) and the particle remains decahedral after it has cooled, (g) 500, (h) 700, (i) 800 (the surface becomes disordered but the underlying crystalline structure remains), (j) 850 K.

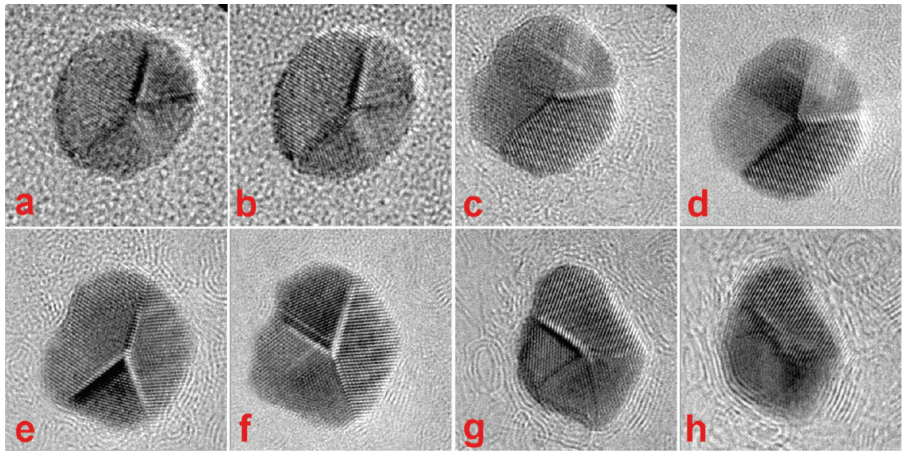

Figure 5. Representative images taken from a series of HRTEM images of a Au nanoparticle as a function of temperature. The average nanoparticle diameter is ~10.3 nm. Initial decahedral structure (close to a ⟨110⟩ projection) at (a) 300 (room temperature), (b) 600, (c) 750, (d) 800 K. (e,f) At 900 K the structure becomes distorted, with significant surface roughening, but retains the underlying crystallinity, (g) 950, (h) 1000 K (crystalline areas are still apparent, though the surface appears almost fluid).

remember that it is a thermodynamic construct and as such is incapable of predicting shapes that result from purely kinetic considerations. From Figure 2 it is apparent that the different motifs are very close in free energy, indicating that transformation can easily result from a suitable kinetic driving force. Moreover, from this figure we can see how it is possible to quantify the *size and temperature regimes* where kinetics will be most important, even though the kinetic effects themselves cannot be quantified using this approach. This may seem undesirable, but it is the very feature that facilitates experimental verification.

EXPERIMENTAL VERIFICATION

Verifying a phase map is a very challenging undertaking. In the present study we have used colloids of gold nanoparticles at various sizes prepared by the reduction of dilute solutions of tetrachloroauric acid, using maltodextrin to prevent aggregation. The samples as prepared contain particles ranging in size from 5 to 12 nm (average diameter), which means that we expect them all to occupy the decahedral region of the phase map at room temperature, and the decahedral-surface roughening transition line is the only testable transition line available to us. Maltodextrin is suitable for use here as its decomposition happens at approximately 400 K, well below the proposed transition temperature, and it is expected that the decomposition reaction will be complete in our high vacuum environment.[19]

Individual nanoparticles were examined using high-resolution transmission electron microscopy (HRTEM) to assign their structure, *during* in situ heating experiments. While transmission electron microscopy images represent a two-dimensional projection of a three-dimensional nanoparticle structure, the high-resolution phase contrast originating from polyhedral metallic nanoparticles of the sizes observed in the current study has been well characterized and understood. It should be noted that a study of smaller nanoparticles, below the size range of applicability of our theoretical model,[14] can be found in ref 20.

To begin with, the as-grown particles presented a range of structural motifs, arising from variations in growth kinetics and solution chemistry. Therefore, the first task was to determine the equilibrium morphology. This was achieved by steadily heating samples in the TEM, from room temperature up to ~700 K, while observing individual particles with a clearly recognizable morphology in projection. Since this increase in temperature provides a sufficient driving force for a morphological transformation (Figure 2) the nanoparticles were able to thermodynamically equilibrate. A statistical analysis of samples surviving[21] heating experiment reveals that 88% of the (equilibrated) nanoparticles exhibited the decahedral structure after heating to 650−700 K, while for 12% of the nanoparticles the as-grown (mainly icosahedral) structure persisted. HRTEM image sequences were collected from data recorded during the heating of 22 samples before the support failed, and in a few cases it was possible to heat, cool, and reheat the same nanoparticle.

The second task was to test the decahedral-surface roughening transformation line. This proved to be an even more challenging exercise, but was achieved for five individual (equilibrated) nanoparticles, heated to *ca.* 800−850 K. A temperature sequence illustrating typical results is given in Figure 4, showing an individual ~7.5 nm gold nanoparticle heated from 300 (room temperature) to 750 K to fully equilibrate the particle, and then cooled back to room temperature. We then reheated the nanoparticle, this time above the predicted surface roughening transition temperature, and Figure 4i shows that at a temperature of 800 K the decahedral structure is ill-defined, although an underlying crystalline "ghost" structure is faintly apparent. This core crystallinity was found to be resilient, as illustrated by another example of a 10.3 nm particle shown in Figure 5e,f. In all but one case the onset of surface melting was measured at ~800 K, which is in excellent agreement with the theoretical prediction (Figure 6).

The final task was to verify the melting and quasi-melting transitions, however we were unable to maintain the integrity of the sample at sufficiently high temperature to achieve this goal. Fortunately a detailed study of the melting of gold nanoparticles has already been undertaken by Koga *et al.*,[22] in which gold nano-

particles were heated above the size-dependent melting temperature and then characterized (postmelting) using HRTEM. On the basis of systematic tests of more than 4000 individual gold nanoparticles (3−4 nm in diameter), the authors undertook a statistical analysis of the results, and were able to predict the relative stability of icosahedral and decahedral motifs just below the melting points.[10] These results are included in Figure 6, where the Δ and ∇ symbols represent the melting temperatures of icosahedral and decahedral structures, respectively.

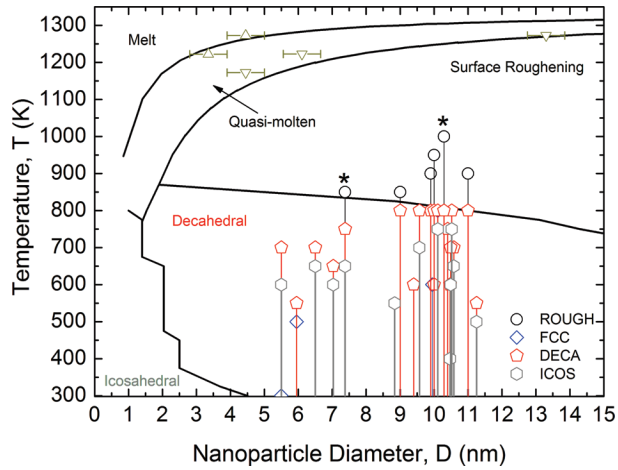

Figure 6. The region of the nanoscale phase map (Figure 3) accessible by our experiments, the experimental observations overlaid. The (isovolumetric) vertical lines represent the heating of individual particles, and the structural motifs (following structural transformation) are indicated by the symbols. The Δ and ∇ symbols represent the melting temperatures of icosahedral and decahedral structures, respectively, measured by Koga *et al*. Reprinted with permission from ref 10. Copyright 2005 American Physical Society. Structures shown in Figures 4 and 5 are indicated with an asterisk.

CONCLUSION

We have presented here the first *quantitative* ⟨*T*,*D*⟩ phase map for gold nanoparticles, based on relativistic *ab initio* calculations. This phase map predicts the stability regime for icosahedral, decahedral, and fcc motifs (as a function of size and temperature), and includes surface roughening and melting transitions. It has been experimentally verified using *in situ* high resolution TEM heating experiments, that provide a record of real-time structural evolution that has never been achieved before. This nanoscale phase map provides unrivaled predictive and explanatory capabilities for understanding the morphology and stability of gold nanoparticles.

The next stage in this study will be to generate a new phase map for gold nanoparticles capped with alkanethiols, with another dimension for degree of monolayer coverage, or chain length. Future plans also include the generation of nanoscale phase maps for other fcc metals such as platinum, palladium, and copper since the principle and methodology described here are immediately applicable.

METHODS

Theoretical Modeling. In the present study, we have used the shape-dependent thermodynamic model developed by Barnard.[14] This model requires input of specific surface free energies, isotropic surface stresses, twin energies and re-entrant line-tensions, which must be calculated explicitly for all facets, twin planes, and re-entrant orientations of interest. Previously all of the critical input parameters needed to describe gold nanoparticles have been calculated at $T = 0$, using scalar relativistic density functional theory within the generalized gradient approximation, and shown to be in excellent agreement with other theoretical studies and experimental results.[14,23,28,29] Therefore, we have opted to use them herein and apply methods based on the work of Guggenheim[24,25] and Qi and Wang[15] to describe the temperature dependence, as described in detail in ref 21.

Synthesis. Gold nanoparticle suspensions were prepared by reducing tetrachloroauric acid ($HAuCl_3$) dilute solutions with different amounts of sodium citrate or mixtures of sodium citrate and tannic acid to get uniform Au nanoparticles of different sizes.[27] To prevent autoaggregation of the concentrated gold nanoparticle suspensions, 2.5% maltodextrin was added to the solution as a stabilizer prior to gold chloride reduction.[26] To obtain uniform Au nanoparticles and reproducible results, all glassware was washed thoroughly with a nonionic detergent followed by copious rinsing with deionized water to remove any dirt that might otherwise nucleate particles and any ionic species that might cause the colloidal suspensions to flocculate by thinning the ionic double-layer surrounding the nanoparticle. The nanocrystals were initially characterized at room temperature using a CM 200 high-resolution TEM operated at 200 kV.

Characterization. High-resolution transmission electron microscopy (HRTEM) was performed on individual isolated Au nanoparticles over a range of elevated temperatures. This was facilitated through drop-casting of dilute colloidal suspension directly onto a novel Si_3N_4-based heating chip.[30] This MEMS micro-hotplate has a low heat capacity and therefore exhibits desirable characteristics such as accurate temperature calibration and low specimen drift. Temperature calibration for the heating control software was performed by heating micro-hotplates inside a vacuum tube furnace and monitoring the temperature of the internal Pt wire heating element. A CM300-UT field-emission gun transmission electron microscope operating at 300 kV was used for *in situ* HRTEM studies. Although the temperature changes of the MEMS micro-hotplates are well controlled by feedback electronics, to within an accuracy of 0.1 K, the overall precision in the absolute temperature once inside the microscope is estimated at ±30 K, due to possible local temperature variations on the substrate and beam-induced heating. HRTEM data was acquired at a primary magnification of around 600 KX. Images were taken using a Tietz fast-scan camera with an exposure of 200 ms, to obtain 512 × 512 pixel images and real-time monitoring of the nanoparticles.

Acknowledgment. The authors would like to gratefully acknowledge financial support from NSF (EAR-0810150), the EPSRC (grant EP/F048009/1), the European Union Framework 6 program under the Integrated Infrastructure Initiative (Reference 026019 ESTEEM), the Royal Society, the ARC (DP0986752), L'Oréal Australia, and the Australian Academy of Sciences. We would also like thank Larry A. Curtiss from Argonne National Laboratory and George D. W. Smith from the University of Oxford for support and useful discussions throughout this project. Henny Zandbergen is acknowledged for assistance and support, with regard to the dedicated specimen heating holder used in this work, designed and constructed in Delft.

Supporting Information Available: Theoretical modeling, computations. This material is available free of charge *via* the Internet at http://pubs.acs.org.

REFERENCES AND NOTES

1. Sperling, R. A.; Rivera Gil, P.; Zhang, F.; Zanella, M.; Parak, W. J. Biological Applications of Gold Nanoparticles. *Chem. Soc. Rev.* **2008**, *37*, 1896–1908.
2. Campbell, C. T. The Active Site in Nanoparticle Gold Catalysis. *Science* **2004**, *306*, 234–235.
3. Elechiguerra, J. L.; Reyes-Gasga, J.; José-Yacamán, M. The Role of Twinning in Shape Evolution of Anisotropic Noble Metal Nanostructures. *J. Mater. Chem.* **2006**, *16*, 3906–3919.
4. Buffat, P.-A.; Flüeli, M.; Spycher, R.; Stadelmann, P.; Borel, J.-P. Crystallographic Structure of Small Gold Particles Studied by High-Resolution Electron Microscopy. *Faraday Discuss.* **1991**, *92*, 173–187.
5. Ino, S. Epitaxial Growth of Metals on Rocksalt Faces Cleaved in Vacuum. II. Orientation and Structure of Gold Particles Formed in Ultrahigh Vacuum. *J. Phys. Soc. Jpn.* **1966**, *21*, 346–362.
6. Marks, L. D. Experimental Studies of Small Particle Structures. *Rep. Prog. Phys.* **1994**, *57*, 603–649.
7. Iijima, S.; Ichihashi, T. Structural Instability of Ultrafine Particles of Metals. *Phys. Rev. Lett.* **1986**, *56*, 616–619.
8. Baletto, F.; Ferrando, R. Structural Properties of Nanoclusters: Energetic, Thermodynamic, and Kinetic Effects. *Rev. Mod. Phys.* **2005**, *77*, 371–423.
9. Link, S.; El-Sayed, M. A. Optical Properties and Ultrafast Dynamics of Metallic Nanocrystals. *Annu. Rev. Phys. Chem.* **2003**, *54*, 331–346.
10. Koga, K.; Ikeshoji, T.; Sugawara, K. Size- and Temperature-Dependent Structural Transitions in Gold Nanoparticles. *Phys. Rev. Lett.* **2004**, *92*, 115507–115517.
11. Kuo, C.-L.; Clancy, P. Melting and Freezing Characteristics and Structural Properties of Supported and Unsupported Gold Nanoclusters. *J. Phys. Chem. B* **2005**, *109*, 13743–13754.
12. Ajayan, P. M.; Marks, L. D. Quasimelting and Phases of Small Particles. *Phys. Rev. Lett.* **1988**, *60*, 585–587.
13. Baletto, F.; Ferrando, R.; Fortunelli, A.; Montalenti, F. Crossover among Structural Motifs in Transition and Noble-Metal Clusters. *J. Chem. Phys.* **2002**, *116*, 3856–3863.
14. Barnard, A. S. A Thermodynamic Model for the Shape and Stability of Twinned Nanostructures. *J. Phys. Chem. B* **2006**, *110*, 24498–24504.
15. Qi, W. H.; Wang, M. P. Size and Shape Dependent Melting Temperature of Metallic Nanoparticles. *Mater. Chem. Phys.* **2004**, *88*, 280–284.
16. Wang, Y; Teitel, S.; Dellago, C. Melting of Icosahedral Gold Nanoclusters from Molecular Dynamics Simulation. *J. Chem. Phys.* **2005**, *122*, 214722–214737.
17. Nam, H.-S.; Hwang, N. M.; Yu, B. D.; Yoon, J.-K. Formation of an Icosahedral Structure During the Freezing of Gold Nanoclusters: Surface-Induced Mechanism. *Phys. Rev. Lett.* **2002**, *89*, 275502–275505.
18. Sutter, P. W.; Sutter, E. A. Dispensing and Surface-induced Crystallization of Zeptolitre Liquid Metal-Alloy Drops. *Nat. Mater.* **2007**, *6*, 363–366.
19. Tomasik, P.; Anderegg, J. W.; Schilling, C. H. Complexes of 3.6 kDa Maltodextrin with Some Metals. *Molecules* **2004**, *9*, 583–594.
20. Li, Z. Y.; Young, N. P.; Di Vece, M.; Palomba, S.; Palmer, R. E.; Bleloch, A. L.; Curley, B. C.; Johnston, R. L.; Jiang, J.; Yuan, J. Three-Dimensional Atomic-Scale Structure of Size-Selected Gold Nanoclusters. *Nature* **2008**, *451*, 46–48.
21. A number of particles examined changed orientation during heating so as to make them unidentifiable. In addition a number of the substrates used fractured during heating.
22. Koga, K.; Sugawara, K. Population Statistics of Gold Nanoparticle Morphologies: Direct Determination by HREM Observations. *Surf. Sci.* **2003**, *529*, 23–35.
23. Barnard, A. S. Modelling the Shape, Orientation and Stability of Twinned Gold Nanorods. *J. Phys. Chem. C* **2008**, *112*, 1385–1390.
24. Guggenheim, E. A. *Thermodynamics*, 4th ed.; North Holland: The Netherlands, 1993.
25. Somorjai, G. A. *Introduction to Surface Chemsitry and Catalysis*; John Wiley & Sons, Inc.: New York, 1994.
26. Hillyer, J. F.; Albrecht, R. M. Gastrointestinal Persorption and Tissue Distribution of Differently Sized Colloidal Gold Nanoparticles. *J. Pharm. Sci.* **2001**, *90*, 1927–1936.
27. Albrecht, R. M.; Simmons, S. R.; Pawley, J. B. Correlative Video-Enhanced Light Microscopy, High Voltage Transmission Electron Microscopy, and Field Emission Scanning Electron Microscopy for the Localization of Colloidal Gold Labels. In *Immunocytochemistry: A Practical Approach*; Beesley, J. E., Ed.; Oxford University Press: New York, 1993; pp 151−176.
28. Barnard, A. S.; Lin, X. M.; Curtiss, L. A. Equilibrium Morphology of Face Centered Cubic Gold Nanoparticles >3 nm, and the Shape Changes Induced by Temperature. *J. Phys. Chem. B* **2005**, *109*, 24465–24472.
29. Barnard, A. S.; Curtiss, L. A. Modeling the Preferred Shape, Orientation and Aspect of Gold Nanorods. *J. Mater. Chem.* **2007**, *17*, 3315–3323.
30. van Huis, M. A.; Kunneman, L. T.; Overgaag, K.; Xu, Q.; Pandraud, G.; Zandbergen, H. W.; Vanmaekelbergh, D. Low-Temperature Nanocrystal Unification Through Rotations and Relaxations Probed by *in Situ* Transmission Electron Microscopy. *Nano Lett.* **2008**, *8*, 3959–3963.